Electron subbands on InP

Hou-Chi Cheng* and F. Koch
Physik-Department, Technische Universität München, 8046 Garching, West Germany
(Received 5 February 1982; revised manuscript received 7 May 1982)

For both *n*- and *p*-type (100) InP surfaces prepared from bulk material, we observe the conductivity of electrons in surface subbands. We report observations regarding the surface layer capacitance and link it with the conduction threshold. After some remarks on the conductivity $\sigma(N_s)$ and the field-effect mobility $\mu_{FE}(N_s)$, we present data on the magnetoconductance $\sigma_{xx}(H,N_s)$ and associated quantum oscillation effects. Two subbands with occupancies N_s^0 and N_s^1 are found for surface densities $N_s > 1\times10^{12}$ cm^{-2}. The measured occupancies allow the construction of the subband splitting $E_1-E_0\equiv E_{01}(N_s)$. We find evidence in InP for an enhanced spin splitting of the Landau levels. A final part of the paper reports on surface cyclotron resonance.

I. INTRODUCTION

The direct-gap semiconductor InP, with gap energy in the light-optical range and with high-electron mobility, has attracted some interest for device applications recently. Metal-insulator-semiconductor (MIS) transistor devices have been fabricated and first results of physical studies of surface electron subbands have appeared in the literature.[1–3]

The present work is a continuation and comprehensive account of the experiments first reported in Ref. 3. For a number of different *n*- and *p*-type, [100]-oriented samples measurements have been made to characterize surface band bending and electron transport in the surface layer. Compared to the intensively studied Si-SiO_2 interface, transport on InP surfaces is largely uncharted territory. Many of the results are likely to depend on the specifics of the preparation of the *I-S* interface. It is essential, in order to understand the properties of the subband electrons, to examine also the interface capacitance and charging characteristics as well as the surface conductance and field-effect mobility. Thus in Sec. III, where we present experimental results, these precede the discussion of magnetoconductance, Shubnikov-de Haas (SdH) oscillations, and surface cyclotron resonance. Section II contains a few brief notes on sample preparation and references on the measurement procedures. In Sec. IV we summarize the physical results.

II. EXPERIMENTAL NOTES

The samples are prepared from (100) wafers, typically 0.5-mm thick. The wafers as purchased have been lapped and polished on one side by the supplier.[4] Prior to the deposition of the insulating layer, the surface is freshly prepared by the following steps: a 30 min etch in 45% KOH solution, immersion in a phosphoric acid–hydrogen peroxide (1:1) polishing bath for 20–30 min, a thorough rinsing in acetone and water. Surfaces that have been damaged by breakdown discharge through the insulator are newly lapped and polished in order to be reused. Our polishing procedure employs conventional mechanical lapping with diamond paste. There follows a chemical polish on a rotating-disk arrangement with bromine-methanol (0.02% Br by volume) solution.

Immediately after preparation of the fresh surface, it is coated with an insulating lacquer layer on a conventional spinner. The technique has been employed also in earlier work on Ge (Ref. 5) and InSb (Ref. 6). Typical thicknesses are $d_{ins}\sim2$ μm. A semitransparent gate electrode of Ni-Cr is evaporated on a rectangular area 4×5 mm^2. The back side is a rough, as-cut surface to which contact is made in order to complete the MIS capacitor structure. The contacts are made by spark discharge of an alloy wire. We use Au-Zn wire for *p*-type InP, and Au-Sn for *n*-type samples.

Quite a few samples were made in this fashion from three types of wafer material. In order to be able to relate the different measurements, we have restricted the discussion and data shown to two specimens of each material. Table I allows a quick identification of the samples and their labels as employed in Sec. III.

The conductivity measurements on the *p*-type MIS capacitor samples are made with the

TABLE I. InP(100) samples.

Sample label	Manufacturer's wafer No., Source	Nominal substrate doping concentration (cm^{-3})
N_1,N_2,N_4	518/R 4 purchased	undoped, n type $1-1.5\times10^{16}$
P_1,P_2	608/R 4 RRE Malvern, Great Britain	Zn doped, p type 1×10^{15}
P_3,P_4	217/R 1 FTZ Darmstadt, Federal Republic of Germany	Zn doped, p type 6×10^{16}

microwave-transmission techniques employed in previous work on Ge and described in Ref. 5. For the degenerate, highly conducting n-type samples (N_1, N_2, and N_4), we make use of contacts placed on the side of the substrate. In this case the conductivity is obtained as a simple two-terminal measurement. Neither the microwave signal nor the latter two-terminal conductance can be expressed directly in terms of a surface-layer conductivity. Lacking adequate calibration, we show the data in terms of arbitrary units. The cyclotron-resonance data is obtained from the change of transmission of the far-infrared radiation of a molecular-laser source. The technique has been employed also in Ref. 5 for Ge. As in the Ge work, a light emitting diode (LED) mounted near the sample, supplies band-gap light of intensity sufficient to create the minority carriers required for the modulation.

III. EXPERIMENTAL RESULTS AND DISCUSSION

A. Capacitance and conduction threshold characterization

The variation of the MIS capacitance with applied gate voltage and the measurement of the onset of channel conductance provide sensitive indication of band bending and charging of the surface layer. They are an essential test for the adequacy of the *I-S* interface preparation. For the present case of samples without source-drain contacts, the capacitance is also a measure of the modulation and surface-charging capability through the substrate contact.

The small signal ac capacitance $\tilde{C}$ in Fig. 1 represents the current in the substrate-gate circuit. $\tilde{C}$ monitors the surface-layer charging and includes the effect of resistances, possibly non-Ohmic, the substrate contact, possible surface-layer paths, and the substrate. The sample as mounted in the wave-guide–light-pipe system, is exposed to thermal-infrared radiation ($\sim$300 K). This provides majority carrier conduction even at $T\sim4.2$ K. It can, in addition, be illuminated by the LED.

Figure 1 shows $\tilde{C}$ observed for a typical p-type sample under various different conditions. The upper curves $\tilde{C}$ apply for a modulation of $2V_{pp}$. With $f_{\rm mod}=39$ Hz at 77 K and the LED on, we record at $+V_G$ the full insulator capacitance. It is the value calculated from the known parameters and agrees with the static $\bar{C}$. The latter is measured from a static $\Delta Q/\Delta V_G$, with ΔV_G equal to an arbitrary voltage step above $+50$ or below -50 V. $\bar{C}$ is the value used to establish the slope of N_s vs V_G relation. At $+25$ V, $\tilde{C}$ drops and continues to decrease at negative V_G. It falls below the $C_{\rm min}$ calculated for the nominal doping level of the sample. The drop below $C_{\rm min}$ increases with a lowering of T below 77 K. At 4.2 K, $\tilde{C}$ for both $\pm V_G$ is much reduced, but the break at $+25$ V remains identifiable.

The lower half of Fig. 1 repeats the 4.2-K curve and demonstrates explicitly how it depends on $f_{\rm mod}$. Lowering the frequency from 39 to 6.3 Hz causes a rise of $\tilde{C}$. A similar rise occurs with an

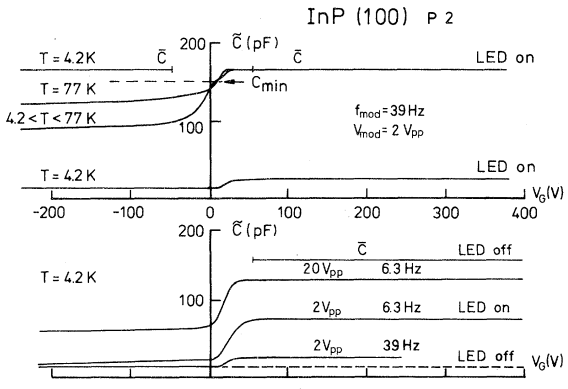

FIG. 1. Dynamic ($\tilde{C}$) and static ($\bar{C}$) capacitances observed under various experimental conditions.

increase of the modulation voltage from 2 to 20 V. The onset of the step in $\tilde{C}$ remains fixed at $+25$ V. The LED illumination is important. With the LED turned off, a small background $\tilde{C}$ is observed for both positive and negative V_G. Since the cable and lead capacitances have been carefully subtracted, the latter must represent a capacitance associated with the sample and its contacts. For LED-off conditions, with large ΔV_G above $+50$ V, one obtains the proper C value for positive V_G.

The complex behavior of $\tilde{C}(V_G)$, which looks unlike the capacitance expected of a p-type sample, results from a great many factors—illumination-induced nonequilibrium, a non-Ohmic substrate contact, possible surface-channel conductivity, interface states, avalanche generation of minority carriers, etc. We do not intend to examine these, but rather to use $\tilde{C}(V_G)$ as an experimental criterion for the onset of surface charging with mobile carriers. We associate the drop of $\tilde{C}$ at $+25$ V with a threshold V_T.

Proof that the drop of $\tilde{C}$ should be identified with V_T is provided in Fig. 2. Curves of $\tilde{C}$ are shown for sample P_3 together with the surface conductivity. Figure 2 also demonstrates that bias stress at room temperature can be used to shift V_T. The middle curve results when the sample is cooled with shorted gate-substrate contacts. For negative V_G stress applied at 300 K for several

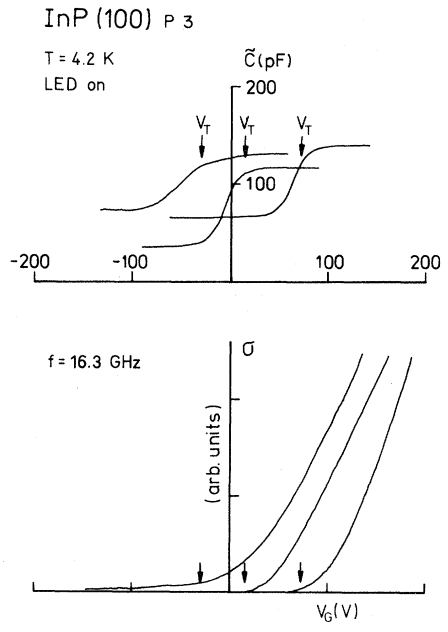

FIG. 2. Correlation of the $\tilde{C}(V_G)$ with the onset of surface conductivity. Voltage prestressing shifts both equally.

hours prior to cooling, V_T is shifted to negative values. Positive prestressing has the opposite effect. The increased rounding of the conductivity onset suggests inhomogeneity of interface charge. The value of $\tilde{C}$ varies with the insulator charge. Because of drift and readjustments of the microwave system, the three conductivity curves cannot be used directly to evaluate differences in the mobility with V_T shift.

The conductivity in Fig. 2 is linked with surface electrons. No surface-hole conductivity is indicated up to the largest negative V_G of 400 V. The distribution of interface states found in Ref. 7 for InP leads one to expect a pinning of the Fermi energy E_F to the conduction-band edge.

In contrast to these observation on the P samples, the n-type specimens show a constant $\tilde{C}(V_G)$ equal to the insulator value. This result would be expected for E_F pinning at the conduction-band edge. Light has no influence on either the surface conductivity or the capacitance.

B. The field-effect mobility μ_{FE}

The variation of the conductivity derivative $d\sigma/dV_G$ with V_G reflects the dependence of scattering on the surface field and charge. It is proportional to what is known as the field-effect mobility μ_{FE}. Under special conditions, structure in $\mu_{Fe}(V_G)$ has been linked with the onset of occupancy of the next higher subband.[8,9]

Figure 3 shows $d\sigma/dV_G$ curves for InP. The upper two traces are σ and $d\sigma/dV_G$ for $N2$, an n-type sample. By and large, after the initial rise, the derivative curve is without distinct features. It remains essentially constant for a well-prepared surface; i.e., the conductivity rises linearly with N_s. Because rounding of the foot of the σ curve makes it difficult to define the onset of conductivity, we use $d\sigma/dV_G$ as an experimentally reproducible criterion for V_T. A straight line is fitted to the rising $d\sigma/dV_G$. Its intercept with the base line for P samples, or with a horizontal line through the background $d\sigma/dV_G$ for N samples, has been used as an operational definition of V_T.

P samples require LED illumination for adequate modulation. For sample P_4 and the lower two traces in the figure, some structure can be identified at the position ($\sim +130$ V) where the magnetoconductance oscillations show the appearance of $n=1$ subband electrons. A dramatic change in the curve occurs after electrical prestressing at room temperature. The broken curve

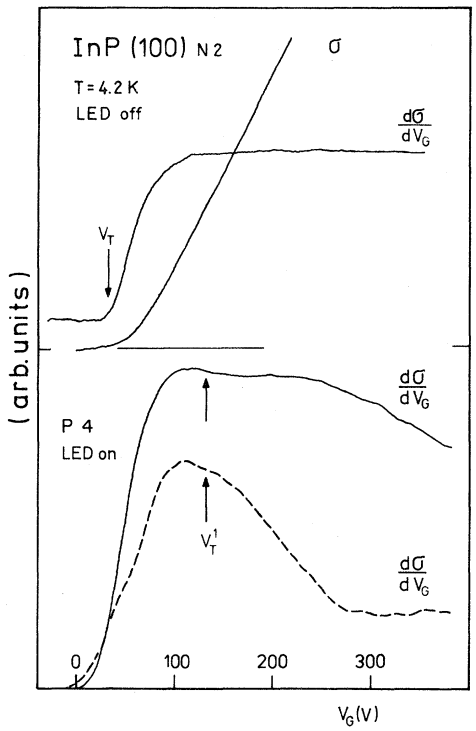

FIG. 3. Mobility curves for n- and p-type samples. The arrow at V_T^1 marks where the next subband is being occupied. The broken line is obtained after a cycle of positive and negative voltage stressing at 300 K.

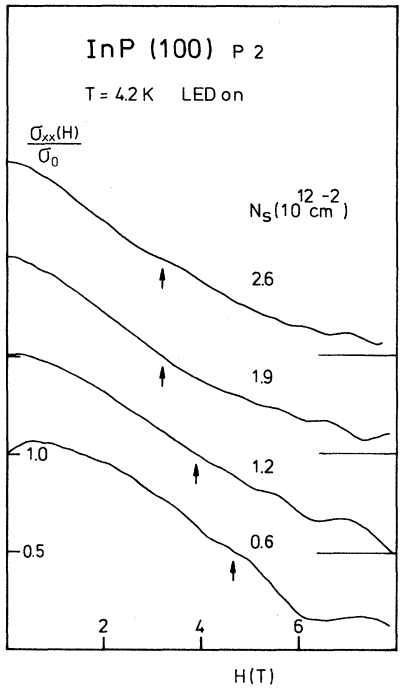

FIG. 4. Conductivity vs magnetic field for different N_s. Successive curves are shifted by 0.5 for clarity. The arrow marks the point $\mu H = 1$.

results after applying $+200$ V for several hours. The change indicates a major reduction of mobility at high N_s. Along with this change in $d\sigma/dV_G$ we observe in SdH measurements a mobility drop for the $n=0$ subband electrons relative to the $n=1$ subband.

C. The magnetoconductivity $\sigma_{xx}(H)$

The variation of the conductivity of p-type specimens in a perpendicular field H provides a convenient measure of the mobility $\mu = e\tau/m^*$. Figure 4 is a set of data for $P2$ when the threshold V_T has been optimized, a procedure which requires cooling down with shorted gate-substrate contacts. The four densities N_s are typical for the range studied.

For all but the lowest N_s, the curves can be fitted well to

$$\sigma_{xx}(H) = \sigma_0/(1+\mu^2 H^2) .$$

The half-amplitude point of σ_{xx}/σ_0 gives $\mu H = 1$. Above 1.5×10^{12} cm^{-2} we obtain a nearly constant $\mu = 3300$ cm^2/V sec. For 1.2×10^{12} cm^{-2}, μ has decreased measurably, and at the lowest density the curve no longer fits the free-carrier relation above. The rising σ at low H is evidence for conduction perturbed by the presence of fixed interface charge. It is most evident at low N_s where screening is poor.

The "negative magnetoresistance" effect can be enhanced dramatically with the V_T shifts that were demonstrated in Fig. 2. Thus after several cycles of drifting forward and backward, the "negative magnetoresistance" effect in sample P_1 was found to exist at all N_s, up to the highest, $\sim 3\times10^{12}$ cm^{-2}. The magnitude, in terms of the rise $\Delta\sigma_{xx}(H)$ $[\equiv \sigma_{xx}^{\max} - \sigma_{xx}(0)]$ divided by $\sigma_{xx}(0)$ exceeded 50% at low N_s. We believe that the effect is related to the negative magnetoresistance discussed in Ref. 10.

D. Quantum-magnetoconductivity oscillations and subband occupation

The curves in Fig. 4, for fields $H > 3.5$ T, show quantum oscillations. The appearance of well-resolved structures is crucially dependent on the V_T. Just how sensitively the oscillations depend on the threshold and related oxide charging is illus-

trated in Fig. 5. With $N_s = 1.5 \times 10^{12}$ cm^{-2} we record $d\sigma/dV_G$ for three settings of V_T. The values of $+70$ and -30 V are achieved with strong positive and negative voltage-bias stressing (at 300 K). $V_T = +14$ V results when the sample is slowly cooled with shorted substrate gate. This results in the highest mobility and good oscillations. Since both of the other threshold settings show substantial rounding of the conductivity onset (compare Fig. 2), we suggest that inhomogeneity of the interface charge contributes to the damping of the oscillations.

With V_T optimized, in a typical P-series sample, the oscillations shown in Fig. 6 are obtained. The evolution of a second period of oscillation with increasing N_s is best followed in this kind of H sweep at fixed N_s. The second period appears clearly resolved only above $N_s = 1.5 \times 10^{12}$ cm^{-2}. It has not been observed in previous work,[3] although the puzzling observation on the irregular spacing of the peaks in an N_s sweep now finds a natural explanation. Two subbands are occupied above $\sim 1 \times 10^{12}$ cm^{-2}. A fan-chart construction is made from data in Fig. 6 with the ordinal numbers assigned as marked.

The densities of occupation N_s^0 and N_s^1 in the first and second subbands are evaluated from the measured periods as $\Delta(1/H) = (e/\pi\hbar)(1/N_s)$. We assume spin degeneracy $g_s = 2$ and a valley factor $g_v = 1$. The sum $N_s^0 + N_s^1$ gives the total density N_s. Generally the N_s^1 electrons are observed down to lower values of the field H. It is possible to deliberately suppress the fast oscillations relative to the long period with the voltage-stressing and V_T-shift procedure.

The oscillations were studied also for N specimens with the use of contacts attached to the sample sides. As in the inset of Fig. 7, the measuring current divides into separate contributions I_B and I_S, through the bulk and surface, respectively. The geometry of current flow is ill defined and, moreover, changes with the field H. The bulk resistance is subject to a large magnetoresistance and carrier freeze out, which results in the steeply rising background of Fig. 7. The oscillatory structure is from the surface layer.

For the N samples, it is preferable to take data using the V_G sweep at constant H. An example is shown in Fig. 8. The conductance oscillations and filling of the $n = 1$ subband appear most clearly in the curves for 2 and 3 T. The onset of occupancy occurs just above $N_S = 1 \times 10^{12}$ cm^{-2}. The general characteristics of the oscillations in N and P samples are surprisingly similar. The evaluation of the SdH periods for N and P samples shows that they

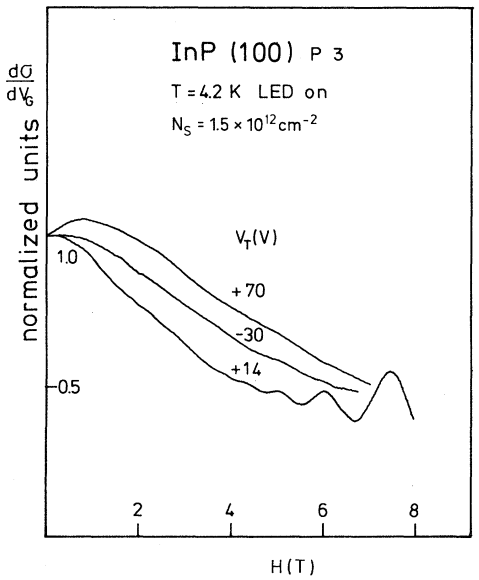

FIG. 5. Effect of threshold V_T on the SdH oscillations.

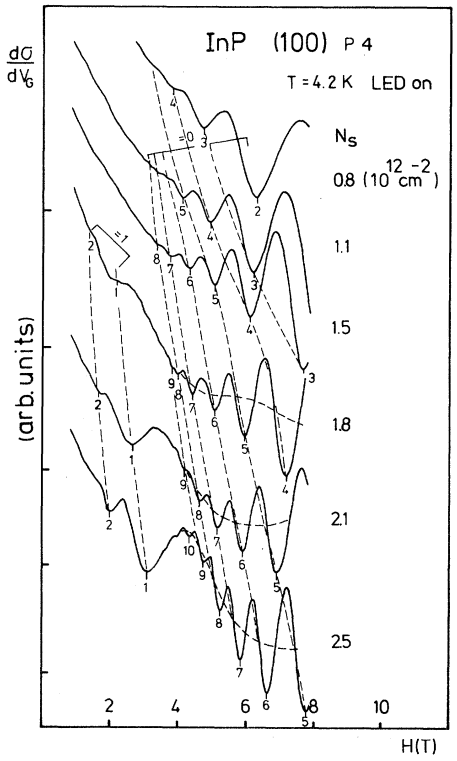

FIG. 6. SdH oscillations in the conductance derivative. At densities $N_s \geq 1.5 \times 10^{12}$ cm^{-2}, a second period is identified.

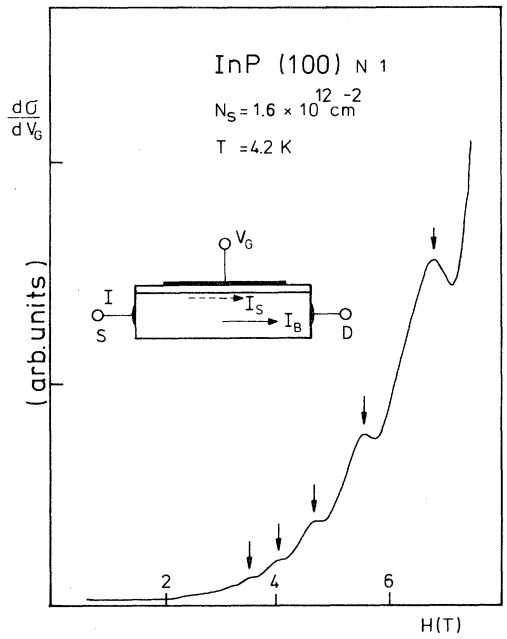

FIG. 7. Oscillations in $d\sigma/dV_G$ vs H for an N sample with S-D contacts.

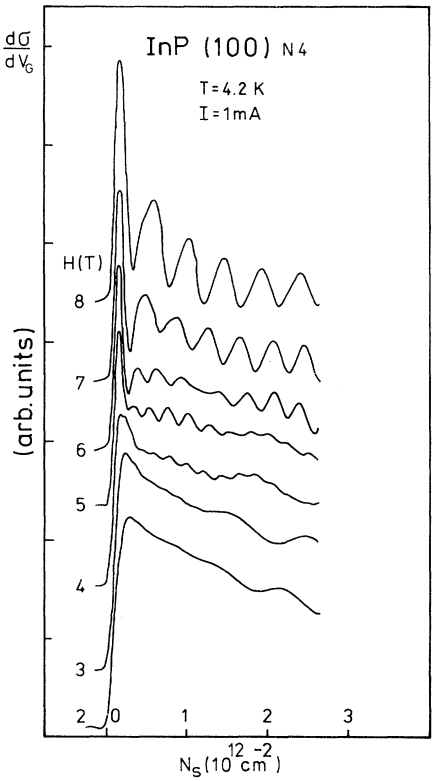

FIG. 8. $d\sigma/dV_G$ vs N_s for an n-type sample.

are identical. We derive the same N_s^0 and N_s^1 for all the three types of material with different magnitude and character of doping.

This result was totally unexpected and allows only one conclusion, namely that we are observing n accumulation on the nominally p-type samples. The occupancies for the three samples P_2, P_4, and N_4 are all plotted in Fig. 9. In each case the sum $N_s^1+N_s^0$ equals the total charge in the surface layer evaluated independently from the capacitance $\bar{C}$ and V_G-V_T. Uncertainties are estimated to be of the order of the size of the points entered in Fig. 9.

A possible reason for the accumulationlike conditions for electrons on P-sample surfaces is the LED illumination. Under band-gap illumination, the depletion charge can be reduced and a quasi-Fermi-level for the minority carriers can rise to near the conduction-band edge. The effect on subbands in Si is well documented. Nevertheless, for InP this is not the case. The proof is obtained with SdH data taken in the absence of band-gap light. Such measurement is made with fixed N_s and employs H modulation in an H sweep. With the sample charged under each of several conditions—V_G applied at 300 K and then cooled down, V_G above avalanche threshold at 4.2 K in the dark, V_G at 4.2 K with LED on at first and then removed, V_G initially above the desired value in the dark and then reduced—we observe identical SdH period in $d\sigma/dH$ with the LED off or on, and in $d\sigma/dV_G$ with LED-on conditions. Both subband periods, with the very same number of charges N_s^0 and N_s^1 as for accumulation on N samples, are observed. We must conclude that the surface layer on all samples is n type. The electrons are always in accumulation subbands.

E. Subband energies

Given the experimentally measured occupancies of two subbands such as N_s^0 and N_s^1, it is a

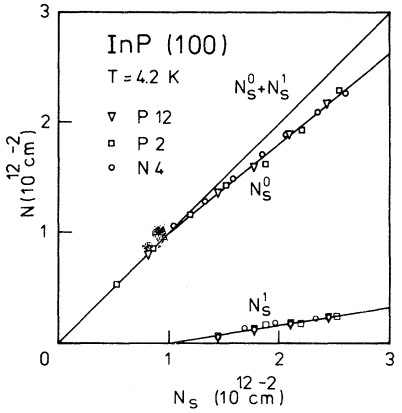

FIG. 9. Subband occupancies N_s^0 and N_s^1 vs total density N_s.

straightforward matter to evaluate a subband-energy separation $E_1 - E_0 \equiv E_{01}$. The density of two-dimensional states for the parabolic band structure of InP is $D(E) = m^*_{||}/(\pi\hbar)$, with $m^* = 0.08 m_0$. It follows from this constant density for each of the subbands that

$$D(E)E_{01} = N_s^0 - N_s^1 .$$

This relation is exploited to construct an experimental E_{01} vs N_s in Fig. 10. The accuracy is as good as that of the occupancy determination. The scatter in the experimental points of Fig. 9 justifies only a straight-line relation for E_{01} in the range of N_s where the two subbands are occupied.

The experimental $E_{01}(N_s)$ is compared with various calculations in the figure. The results of Kawamoto *et al.*[11] and v. Klitzing *et al.*[2] apply for inversion with the depletion charge as marked. The N_{dep} is near that expected for the nominal doping level of samples P_3 and P_4. The triangular points are values calculated by Das Sarma for accumulation and in the absence of many-body effects.[12] Tränkle[13] has independently calculated for us the accumulation case including exchange and correlation in density-functional approximation. The agreement of the experimental E_{01} with the accumulation case provides additional confirmation that there is an *n*-type surface layer on the *p*-type samples.

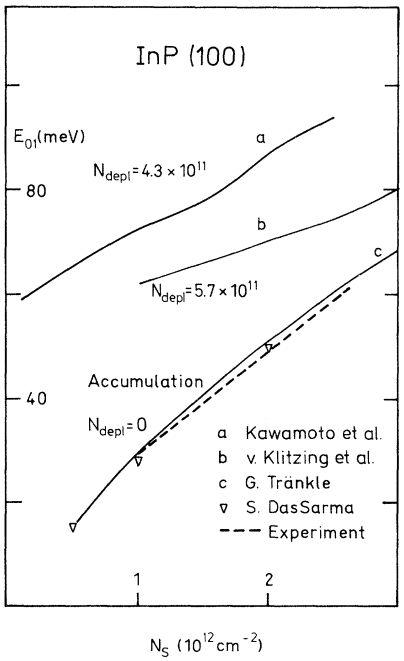

FIG. 10. Subband energy splitting E_{01} vs N_s.

F. Spin splitting

An unexpected feature of the oscillations is the appearance of additional structure in the very highest mobility samples and with optimally adjusted V_T. In high magnetic field the peaks are split, thus removing the only remaining twofold spin degeneracy. The effect can be seen at 4.2 K in the accompanying Fig. 11 for $H = 8$ T. With the temperature reduced, the splitting is enhanced and can be followed down to about 5 T in sample N_2. Figure 11, in particular, demonstrates how sensitive the effect is to the magnitude of the sample current. Since for the microwave-type measurement in *P* samples the necessary power level is relatively high, the splitting is not observed there. The complicated geometry of current flow in the *N* samples does not permit a quantitative evaluation of the power dissipated in the surface layer for the data in Fig. 11. The dependence on the total sample current is only a qualitative measure.

We suggest that spin is the reason for the splitting, because it is the one degeneracy that still remains in the description of the surface electrons. Nevertheless, a simple estimate of the spin energy $g_s \mu_B H$, with $g_s = 1.26$ and $H = 8$ T, gives ~ 0.6 meV which is much less than the Landau-level broadening. The latter we can estimate from the mobility. Taking our clues from the magnetoconductivity in Fig. 4, we expect that $\omega_c \tau \approx 2$ at 8 T, where the Landau splitting $\hbar\omega_c \sim 12$ meV. It follows that the broadening is of the order of 6 meV. The ratio of spin energy to level width is therefore of the order of 0.1 when the splitting is resolved.

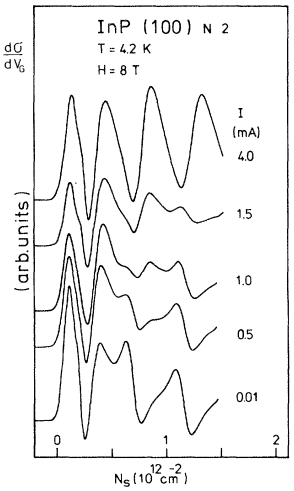

FIG. 11. Dependence of the anomalous splitting on the total measuring current *I*.

The result is surprising, but it is in line with what has been observed and examined in detail for GaAs.[14] The splitting has been explained there in terms of an exchange energy effect, which acts to enhance the spin splitting energy.

G. Surface cyclotron resonance

The resonance absorption of the surface carriers at infrared frequencies in a perpendicular magnetic field has been used to obtain the effective mass and scattering time for surface layers on Si (Refs. 15 and 16) and various other semiconductors. Judging from the magnetoconductivity described earlier, we expect that $\omega_c\tau\sim 2$ at 8 T and for the infrared energy ~ 12 meV. Thus cyclotron-resonance experiments on InP should be possible.

The N samples are degenerate and opaque at the frequencies of interest in zero field. In transmission cyclotron experiments, one observes both magnetoplasma-edge behavior and carrier freeze out from the volume. This complicates and interferes with the interpretation of the surface-layer absorption. In addition, several magnetoimpurity resonances give sharp structures in both direct transmission and in the surface-modulated mode. We restrict the present discussion for this reason to work with P-series specimens.

Typical of the results is the set of traces in Fig. 12, where the decrease of transmission of 10.5-meV radiation is recorded as a function of the perpendicular H field for various surface-electron concentrations. As in the previous work on Si,[15] this is recorded in terms of power absorbed in the sample. The signals are obtained with unpolarized radiation and the amplitude never exceeds about 10% of the transmission. Because of difficulties with reflections and standing-wave behavior in parts of the sample holder and apparatus, the amplitudes cannot be quoted reliably in terms of the percentage change of transmission. The origin of each successive curve is shifted by the amount indicated in the lower left of the figure.

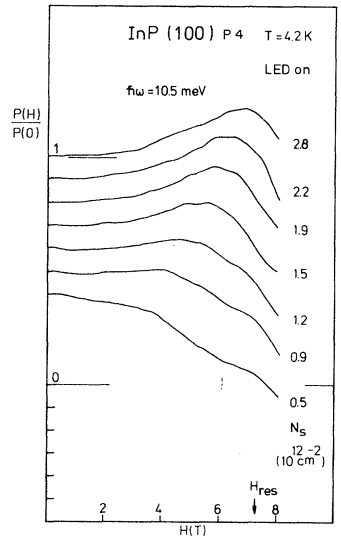

FIG. 12. Surface-cyclotron-resonance absorption $P(H)$ normalized to absorption in zero field. The curves at various densities N_s are offset for clarity.

The resonance line shapes in Fig. 12 are anomalous. The absorption signal is not at all that of free electrons with an $\omega_c\tau\sim 2$. The expected maximum absorption, at $H_{\rm res}$ for the known m_c^* value of $0.08m_0$, is ~ 2.5 times the absorption $P(0)$. Line-shape distortions from interference effects in the sample substrate[15] can be discounted because of the rough, as-cut back surface. Moreover, neither a different choice of $\omega_c\tau$, nor standing-wave interference can account for the radical change of the curves with lowering of N_s. The fact is that this line shape cannot be fit to simple Drude theory of absorption in a magnetic field. The resonance peak, for the highest N_s, falls measurably below $H_{\rm res}$. The cyclotron absorption that is observed here is quite similar to signals in Si at low N_s.[17] There the effect has been linked with perturbation of the surface carriers in a localization potential. It has been qualitatively interpreted in terms of a lowering of the m_c^* in a Drude description.

According to a model description[18] of the perturbed surface cyclotron resonance, the resonance should approach free-electron behavior as the energy of excitation is raised in relation to the surface-localization potentials. That this is the case here we demonstrate in the final Fig. 13. The data for p_4 are repeated at $\hbar\omega=12.9$ meV. The resonance maximum is now more clearly identifiable and for the same N_s nearer the expected $H_{\rm res}$. The curves for $N_s<1\times 10^{12}$ now show up a maximum. Figure 13 also has chosen data taken with a lower temperature in order to demonstrate the existence of the quantum oscillations in the transition probability as predicted by Ando[19] and studied in detail for Si in Ref. 15.

IV. CONCLUSIONS

In this final section we provide a brief overview of the knowledge that has been gained about the

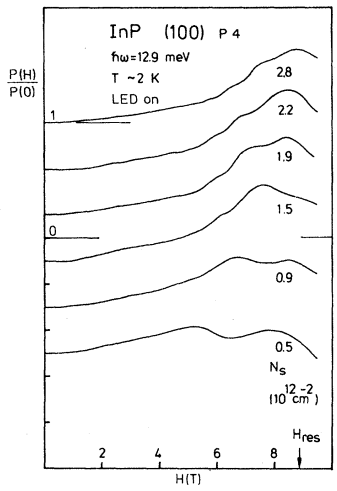

FIG. 13. Surface-cyclotron resonance with $\hbar\omega = 12.9$ meV. Compare with the preceding figure for $\hbar\omega = 10.5$ meV.

physical properties of electron transport on surfaces of InP.

The routines of surface oxidation that provide for Si an easily reproducible and well-characterized *I-S* interface, are not available for InP. It follows that a number of the results in the previous sections are tied to the specific chemical and physical preparation procedures that we have employed. The chemical polishing and the room-temperature deposition of a chemically inert lacquer insulator have in this work yielded samples that differ markedly from those prepared for the investigations of v. Klitzing *et al.* in Ref. 2. The most striking difference is the ~six times higher surface mobility that is achieved here.

After this word of caution about interface preparation, here are the facts, features, and conclusions as they relate to the InP *MIS* structures employed in this study. The *MIS* capacitance of *n*-type samples is constant and equal to the insulator value. That of the *P* samples varies with V_G in an unusual and not easily understood manner. There is a marked drop of the dynamic capacitance when the V_G is lowered. The drop is linked in Fig. 2 to the disappearance of surface *n*-channel conduction and thus provides an easy identification of the threshold voltage V_T. In both types of specimens, the Fermi level is pinned at the surface in such manner that *p*-channel conduction is never achieved (up to $N_s = 4\times10^{12}$ cm^{-2}). The field-effect mobility variation with V_G has a form that appears superficially similar to Si. It is sensitive to the creation of interface and oxide charge (Fig. 3) primarily at high N_s. The quantitative evaluation of magnetoconductivity data (Fig. 4) gives the transport mobility of good surfaces as 3300 cm^2/V sec. The optimal values achieved in Ref. 2 are only ~500 cm^2/V sec. The observability of strong quantum oscillations in the present samples is tied to reduction of the interface charge (Fig. 5). Two periods of oscillation from two occupied surface bands are identified for $N_s > 1\times10^{12}$ cm^{-2} (Figs. 6 and 8). The occupancies and energy splitting of the $n=0$ and $n=1$ subbands have been determined (Figs. 9 and 10).

The comparison of the energy with theory leaves no doubt that the surface electrons on both *p*- and *n*-type specimens are in an accumulationlike potential well, i.e., the surface layers prepared in this work are always *n* type, independent of substrate doping. The occupation of two subbands is a consequence of the accumulation conditions. Accumulation is also one reason for the high mobility. The work in Ref. 2 shows a decrease of mobility with rising depletion field. There is observed a twofold splitting of the oscillation peaks (Fig. 11) for the highest mobility samples at low values of the surface-current density. We suggest this to be caused by exchange-enhanced spin splitting. Finally, the surface-cyclotron resonance (Figs. 12 and 13) with its deviation from a free-electron-like $\sigma(\omega,H)$ demonstrates explicitly that there are perturbations of the interface conduction. The frequency dependence of the resonance (compare Figs. 12 and 13) is that expected from a model description of cyclotron resonance in the presence of attractive surface potentials.

This paper on InP is a modest first step in understanding electrons at Si-SiO_2 interfaces and GaAs-$Ga_{1-x}Al_xAs$ heterojunctions. Nevertheless, a close comparison with other papers on the same subject is warranted when it comes to cyclotron-resonance results, the spin-splitting effect, and mobility variation with interface fixed charge. We have tried to include many different observations on the same specimen into a single experimental report to allow the interested reader to relate the information contained therein.

V. ACKNOWLEDGMENTS

We have enjoyed an active interaction with a number of research groups concerned with work on interfaces of InP. Helpful discussions with D. Fritzsche of the Fernmeldetechnische Zentrale (FTZ), Darmstadt, with J. Woodward of the Royal

Radar Establishment (RRE), Malvern, and with K. v. Klitzing of our laboratory are gratefully acknowledged. The work was financially supported by the Deutsche Forschungsgemeinschaft (DFG) in the scientific program of the Sonderforschungsbereich (SFB) 128. One of us (H. -C. C.) acknowledges support from the A. von Humboldt Foundation.

---

*Permanent address: Institute of Semiconductor Physics, Academia Sinica, Peking.

[1]D. L. Lile, D. A. Collins, L. G. Meiners, and L. Messick, Electron. Lett. 14, 657 (1978); D. Fritzsche, in *Insulating Films on Semiconductors—1979,* edited by G. G. Roberts and M. J. Morant (Institute of Physics, Bristol, 1980), p. 258.

[2]K. v. Klitzing, Th. Englert, and D. Fritzsche, J. Appl. Phys. 51, 5893 (1980); K. v. Klitzing, Th. Englert, E. Bangert, and D. Fritzsche, *Proceedings of the 15th International Conference on the Physics of Semiconductors, Kyoto 1980* [J. Phys. Soc. Jpn. 49, Suppl. A, 979 (1980)].

[3]H. C. Cheng and F. Koch, Solid State Commun. 37, 911 (1981).

[4]Crystals grown by Metals Research Co., Melbourn Royston, Great Britain.

[5]J. Binder, K. Germanova, A. Huber, and F. Koch, Phys. Rev. B 20, 2382 (1979); 20, 2391 (1979).

[6]W. Beinvogl and F. Koch, Solid State Commun. 24, 687 (1977).

[7]H. Hasegawa and T. Sawada, *Proceedings of the 15th International Conference on the Physics of Semiconductors,* Ref. 2, p. 1125.

[8]I. Eisele, Surf. Sci. 73, 315 (1978).

[9]A. Kastalsky and F. F. Fang, Surf. Sci. 113, 153 (1982).

[10]I. Eisele and G. Dorda, Phys. Rev. Lett. 32, 1360 (1974).

[11]G. H. Kawamoto, J. J. Quinn, and W. L. Bloss, Phys. Rev. B 23, 1875 (1981).

[12]S. Das Sarma, Solid State Commun. 41, 483 (1982).

[13]G. Tränkle, Diplom thesis, Techn. University München, 1981 (unpublished).

[14]Th. Englert, D. C. Tsui, A. C. Gossard, and Ch. Uihlein, Surf. Sci. 113, 296 (1982).

[15]G. Abstreiter, J. P. Kotthaus, F. Koch, and G. Dorda, Phys. Rev. B 14, 2480 (1976).

[16]R. J. Wagner, T. A. Kennedy, B. D. McCombe, and D. C. Tsui, Phys. Rev. B 22, 945 (1980).

[17]J. P. Kotthaus, G. Abstreiter, F. Koch, and R. Ranvaud, Phys. Rev. Lett. 34, 151 (1974).

[18]H. J. Mikeska, and H. Schmidt, Z. Phys. B 20, 43 (1975).

[19]T. Ando, J. Phys. Soc. Jpn. 38, 989 (1975).